The nonlinear evolution of a single mode of the magnetic shearing instability

Ulf Torkelsson[1], Gordon I. Ogilvie[1], Axel Brandenburg[2], Åke Nordlund[3], Robert F. Stein[4]

[1] Institute of Astronomy, Madingley Road, Cambridge CB3 0HA, United Kingdom
[2] Department of Mathematics, University of Newcastle upon Tyne, NE1 7RU, United Kingdom
[3] Theoretical Astrophysics Center, Juliane Maries vej 30, DK-2100 Copenhagen Ø, Denmark
[4] Department of Physics and Astronomy, Michigan State University, East Lansing, MI 48824, USA

Abstract We simulate in one dimension the magnetic shearing instability for a vertical magnetic field penetrating a Keplerian accretion disc. An initial equilibrium state is perturbed by adding a single eigenmode of the shearing instability and the subsequent evolution is followed into the nonlinear regime. Assuming that the perturbation is the most rapidly growing eigenmode, the linear theory remains applicable until the magnetic pressure perturbation is strong enough to induce significant deviations from the original density. If the initial perturbation is not the fastest growing mode, the faster growing modes will appear after some time.

1 Introduction

Balbus and Hawley (1991) realised that a Keplerian accretion disc penetrated by a vertical magnetic field is unstable to a shearing instability previously described by Velikhov (1959) and Chandrasekhar (1960). Three-dimensional numerical simulations (e.g. Hawley et al. 1995, 1996; Matsumoto & Tajima 1995; Brandenburg et al. 1995, 1996; Stone et al. 1996) have later demonstrated that the laminar shear flow becomes turbulent in the nonlinear domain.

Owing to the complexity of a three-dimensional simulation it is not well understood how the flow evolves from being linearly unstable to being turbulent. A related problem is to identify the saturation mechanism that sets the amplitude of the fully developed turbulence. In this paper we will try to investigate these problems in an alternative way. We will reduce the amount of data by studying the instability of a vertical magnetic field in only one dimension, and simplify the dynamics by starting from a perturbation which is already an eigenmode of the linear stability problem. Clearly we are missing much of the essential physics by imposing these restrictions, but on the other hand it is possible to understand the remaining physical effects, and by comparing our results with more complete calculations we may understand which of the missing physical effects are important.

Since the initial analysis by Balbus & Hawley (1991) a large number of papers extending the linear analysis have been published. The original work was generalised by Balbus & Hawley (1992a) who showed that the maximum growth rate of the magnetic shearing instability for any poloidal field configuration is given by Oort's A-constant. A more detailed analysis determining the axisymmetric eigenmodes for a stratified disc was later published by Gammie & Balbus (1994).

The original work concerned only the instability of an axisymmetric poloidal magnetic field, but Balbus & Hawley (1992b) extended the analysis to toroidal fields and non-axisymmetric perturbations. Several groups have later continued the analytical stability analysis of the toroidal field (e.g. Foglizzo & Tagger 1995, Ogilvie & Pringle 1996, Terquem & Papaloizou 1996, Coleman et al. 1995). An important difference in the stability properties of vertical and toroidal magnetic fields is that for the vertical magnetic field the most rapidly growing mode always has a finite wavelength, if there are any unstable modes at all, whereas for a toroidal field the most rapidly growing mode has an arbitrarily small vertical wavelength.

In this paper we will introduce briefly the linear theory for instabilities of a vertical magnetic field in an unstratified disc in Sect. 2, and present the corresponding nonlinear simulations in Sect. 3. Sect. 4 is devoted to magnetic fields in a stratified disc. Finally we summarise and discuss our results in Sect. 5.

2 The linear stability of a vertical magnetic field

The equations of ideal magnetohydrodynamics (MHD) can be written as

$$\frac{\partial \rho}{\partial t} + \nabla \cdot (\rho \mathbf{u}) = 0, \tag{1}$$

$$\frac{\partial \mathbf{u}}{\partial t} + \mathbf{u} \cdot \nabla \mathbf{u} = -\frac{1}{\rho} \nabla p + \frac{1}{\mu_0 \rho} (\nabla \times \mathbf{B}) \times \mathbf{B} + \mathbf{g}, \tag{2}$$

and

$$\frac{\partial \mathbf{B}}{\partial t} = \nabla \times (\mathbf{u} \times \mathbf{B}), \tag{3}$$

where ρ is the density, $\mathbf{u}$ the velocity, p the pressure, μ_0 the magnetic permeability, $\mathbf{B}$ the magnetic field, and $\mathbf{g}$ the gravity. Furthermore we assume an ideal equation of state and that all perturbations are adiabatic. For the rest of this paper we will assume dimensionless units such that $\mu_0 = 1$.

As our equilibrium model we choose a Keplerian accretion disc with no stratification. We transform the equations to a system rotating at the Keplerian angular velocity, Ω_0, at a reference radius R_0, and linearise the shear flow in terms of the parameter $\frac{x}{R_0}$, where x is the radial distance from R_0 (cf. Brandenburg et al. 1995). On this disc we impose a homogeneous vertical magnetic field B. We then add a perturbation of the form $\propto \exp[i(k_z z - \omega t)]$, that is the perturbations

are independent of the horizontal coordinates x and y. Linearising Eqs (2) and (3) we then obtain

$$-\rho\left(i\omega\delta u_x + 2\Omega_0\delta u_y\right) = ik_z B\delta B_x, \tag{4}$$

$$\rho\left[-i\omega\delta u_y + 2\left(\Omega_0 - A\right)\delta u_x\right] = ik_z\delta B_y, \tag{5}$$

$$-\rho i\omega\delta u_z = -ik_z\delta\Pi + ik_z B\delta B_z, \tag{6}$$

$$-i\omega\delta B_x = ik_z B\delta u_x, \tag{7}$$

$$-i\omega\delta B_y = ik_z B\delta u_y - 2A\delta B_x, \tag{8}$$

and

$$-i\omega\delta B_z = 0, \tag{9}$$

where $\delta\Pi = \delta p + \mathbf{B}\cdot\delta\mathbf{B}$ is the perturbation of the total pressure, and

$$A = \frac{1}{2}\left(\Omega - \frac{\mathrm{d}\left(R\Omega\right)}{\mathrm{d}R}\right)_{R_0} \tag{10}$$

is Oort's constant, which is $\frac{3}{4}\Omega_0$ for Keplerian rotation. Note that Eq. (9) leads to $\delta\Pi = \delta p$. The pressure and density perturbations are related via

$$\delta p = v_\mathrm{s}^2\delta\rho, \tag{11}$$

where v_s is the sound speed, and the density perturbation in its turn is given by

$$-i\omega\delta\rho = -i\rho k_z\delta u_z. \tag{12}$$

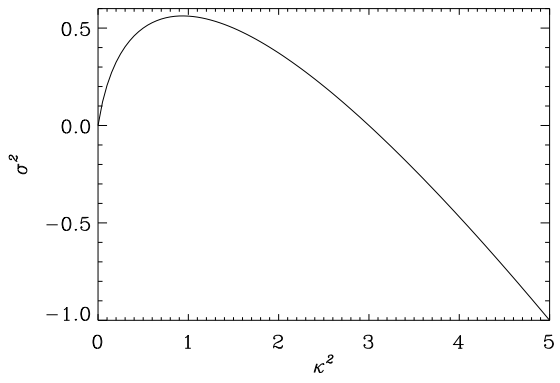

Fig. 1. The dispersion relation for an unstratified disc. κ is a normalised wave number and σ is the growth rate normalised to the Keplerian frequency

The resulting dispersion relation can be split into two parts

$$\omega^2 = v_{\rm s}^2 k_z^2, \tag{13}$$

for longitudinal, 'acoustic', waves, and

$$\omega^4 - \left(2\omega_{\rm A}^2 + \Omega_0^2\right)\omega^2 + \omega_{\rm A}^2\left(\omega_{\rm A}^2 - 3\Omega_0^2\right) = 0, \tag{14}$$

for transverse, 'magnetic' and 'inertial', perturbations. We have defined the Alfvén frequency $\omega_{\rm A} = k_z v_{\rm A}$ for the Alfvén velocity, $v_{\rm A} = B/\sqrt{\rho}$. The magnetic mode is unstable for $0 < \omega_{\rm A}^2 < 3\Omega_0^2$. We now introduce the conditions

$$\frac{\partial u_x}{\partial z} = \frac{\partial u_y}{\partial z} = u_z = 0, \tag{15}$$

and

$$B_x = B_y = \frac{\partial B_z}{\partial z} = 0 \tag{16}$$

on the vertical boundaries. These boundary conditions are identical to the ones used by Brandenburg et al. (1995), and describe a stress-free surface with no flow going through it and with a vertical magnetic field. The unstable magnetic mode can be written as

$$\delta u_x = a, \tag{17}$$

$$\delta u_y = \frac{\sigma^2 + \kappa^2}{2\sigma} a, \tag{18}$$

$$\delta B_x = \frac{i\kappa}{\sigma}\rho^{1/2} a, \tag{19}$$

$$\delta B_y = \frac{i\kappa}{\sigma}\frac{\sigma^2 + \kappa^2 - 3}{2\sigma}\rho^{1/2} a, \tag{20}$$

and

$$\delta u_z = \delta B_z = \delta\rho = \delta p = 0, \tag{21}$$

where a is an arbitrary constant, and κ and σ are given by

$$\kappa = \frac{k_z v_{\rm A}}{\Omega_0}, \tag{22}$$

and

$$\sigma^2 = \frac{1}{2}\left(1 + 16\kappa^2\right)^{1/2} - \left(\frac{1}{2} + \kappa^2\right), \tag{23}$$

respectively (Fig 1), and $\omega = i\sigma\Omega_0$. The instability appears for $\kappa^2 < 3$, and the fastest growing mode has

$$\kappa^2 = \frac{15}{16} \tag{24}$$

so that the dispersion relation reduces to

$$\sigma^2 = \frac{9}{16}. \tag{25}$$

The maximum growth rate is thus equal to Oort's A-constant. The corresponding eigenmode can be written as

$$\delta u_x = \delta u_y = a, \tag{26}$$

and

$$\delta B_x = -\delta B_y = \frac{\sqrt{15}}{3} i \rho^{1/2} a. \tag{27}$$

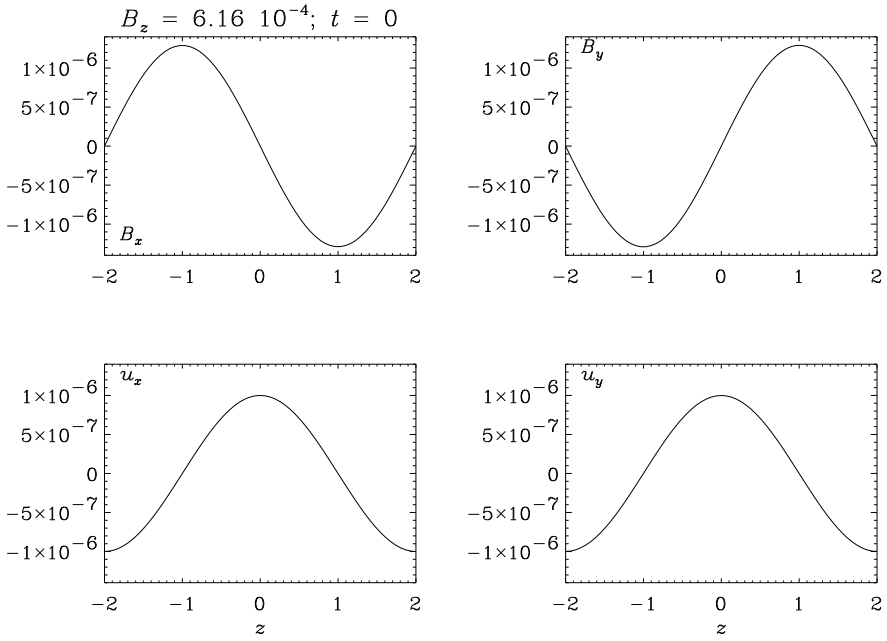

Fig. 2. The initial state of Model 1. The imposed vertical magnetic field is $6.16\,10^{-4}$, the density is 1.0 and the angular velocity is 10^{-3}. The magnetic perturbation is shown in the upper row, and the velocity perturbation in the lower row (x-components to the left and y-components to the right)

3 The evolution of a single mode in an unstratified disc

We use the numerical code of Brandenburg et al. (1995), but restrict it to one dimension, the vertical, to study the evolution of the eigenmodes described above. Our standard background model assumes an initial density $\rho = 1$, a radius of 100, so that $\Omega_0 = 10^{-3}$, and the internal energy, $e = 7.5\,10^{-7}$. The vertical

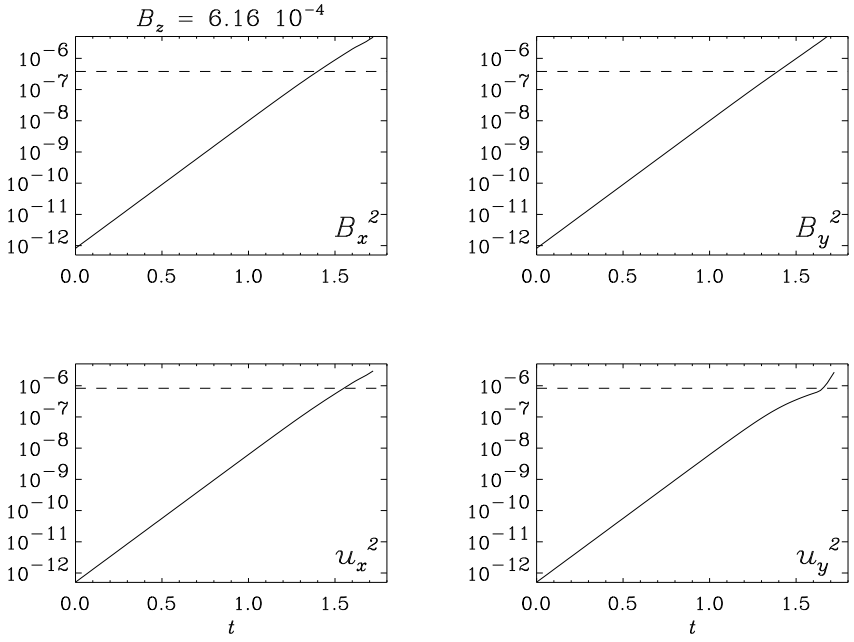

Fig. 3. The vertical averages of B_x^2 and B_y^2 (upper row), and u_x^2 and u_y^2 (lower row) as a function of time for Model 1. Time is given in orbital periods. The dashed lines denote B^2 (upper row) and c_s^2 (lower row)

Table 1. Vertical eigenmodes in unstratified discs. For each model we give the number of grid points used, N_z, the imposed vertical magnetic field, B, the wavelength of the excited mode, λ, and its growth rate, σ in units of the Keplerian angular frequency

Model	N_z	B	$\lambda = 2\pi/k_z$	σ
1	63	$6.16\,10^{-4}$	4	0.75
2	127	$1.54\,10^{-4}$	1	0.75
3	63	$1.54\,10^{-4}$	4	0.37

extent of the box is 4. The eigenmodes that we study are given in Tab. 1. λ is the wavelength of the linear eigenmode of the shearing instability. Models 1 and 2 are the fastest growing eigenmodes for their magnetic field strengths.

The initial state of Model 1 is shown in Fig. 2. The instability is growing at its linear growth rate even in what could be considered to be the nonlinear regime, as is illustrated in Fig. 3. This is a consequence of the fact that the linear

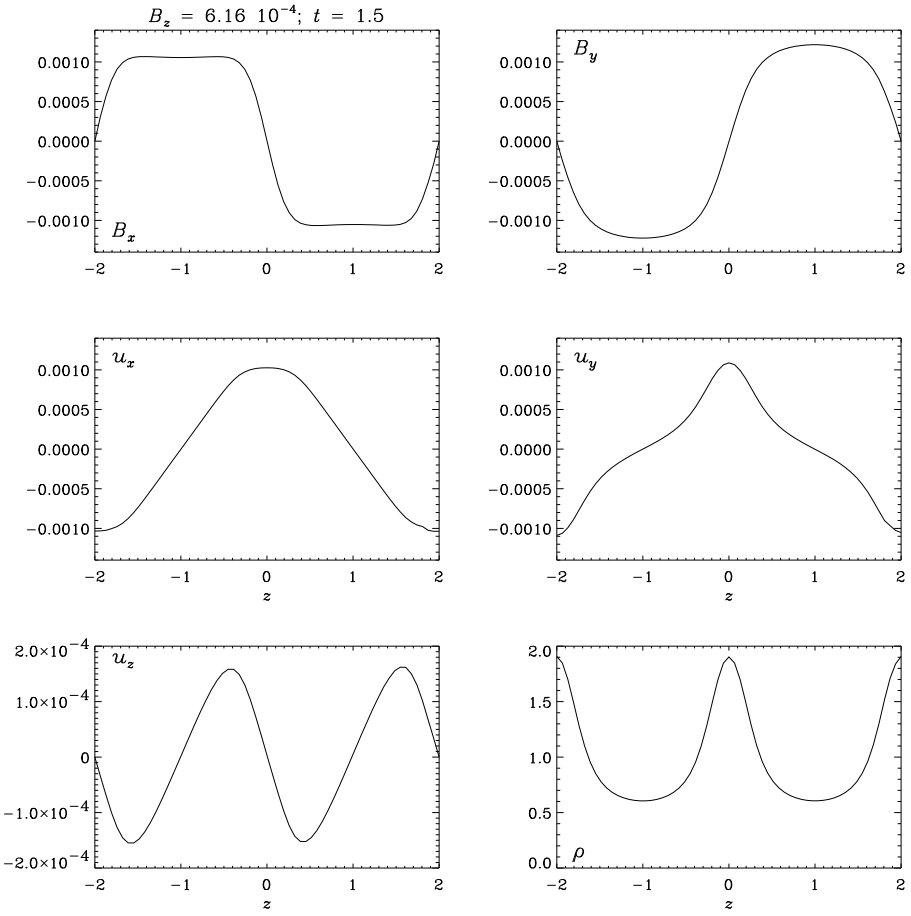

Fig. 4. The evolved state of Model 1 at 1.5 orbital periods. *Upper row*: B_x and B_y. *Middle row*: u_x and u_y. *Lower row*: u_z and ρ. Note that initially $\rho = 1$ and $v_{\rm s} = 9.1\,10^{-4}$

eigenmode is an exact solution of the incompressible MHD equations (Goodman & Xu 1994). It is clear from Fig. 2 that to second order the magnetic pressure is modulated on half the wavelength of the eigenmode. The magnetic pressure gradient generates a vertical velocity, u_z, and a density fluctuation. These effects are of no consequence for the growth of the eigenmode until the density fluctuations are comparable to the background density (Fig. 4). At this late stage the mass is concentrated towards the nodes of the horizontal magnetic field as predicted by Goodman & Xu (1994) when the magnetic pressure dominates over the gas pressure.

Model 2 shows a similar pattern to Model 1, as it is the fastest growing

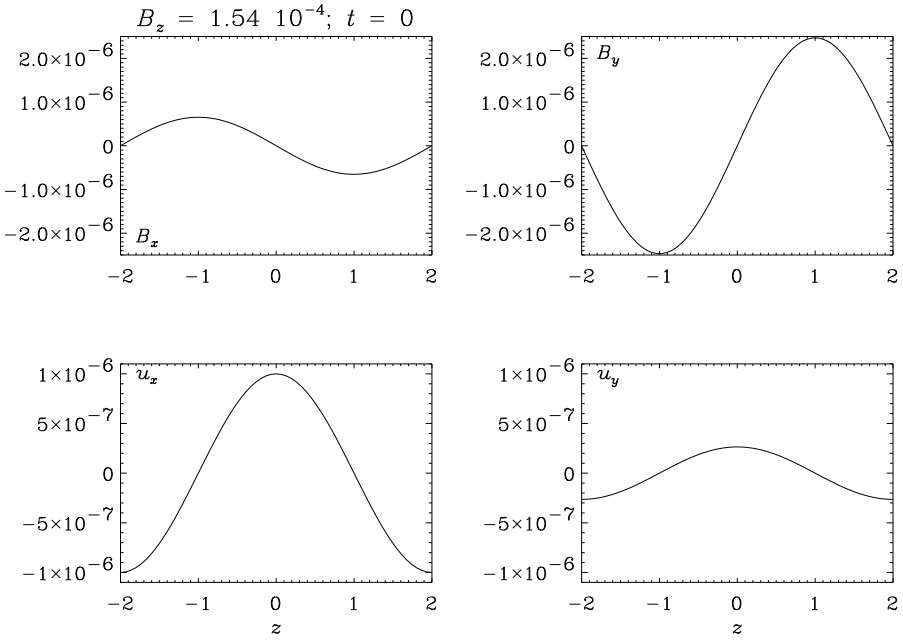

Fig. 5. The initial state of Model 3. The imposed vertical magnetic field is $1.54\,10^{-4}$. The figure is organised in the same way as Fig. 2

mode for that magnetic field strength. Model 3 has the same imposed vertical magnetic field as Model 2, but the eigenmode has a longer wavelength, and thus a lower growth rate. In general $|u_x| > |u_y|$ and $|B_x| < |B_y|$ for a mode with a wavelength longer than that of the fastest growing mode (Fig. 5), and the other way around for a mode with a too short wavelength. The nonlinear terms in the MHD equations transfer power to modes with smaller wavelengths. In Models 1 and 2 these deviations are visible only in quantities which lack a contribution from the linear mode, such as u_z, but in Model 3 the deviations appear in all quantities as they belong to modes with larger growth rates (Fig. 6).

4 A single mode in a stratified disc

We assume a vertical gravitational acceleration $g_z = -\Omega_0^2 z$ and that the disc is isothermal in the vertical direction, so that hydrostatic equilibrium gives

$$\rho = \rho_0 \mathrm{e}^{-z^2/H^2}, \tag{28}$$

where ρ_0 is the density at the midplane of the disc, and H is the scale height. For our standard model we choose both ρ_0 and H to be unity. In this case the vertical

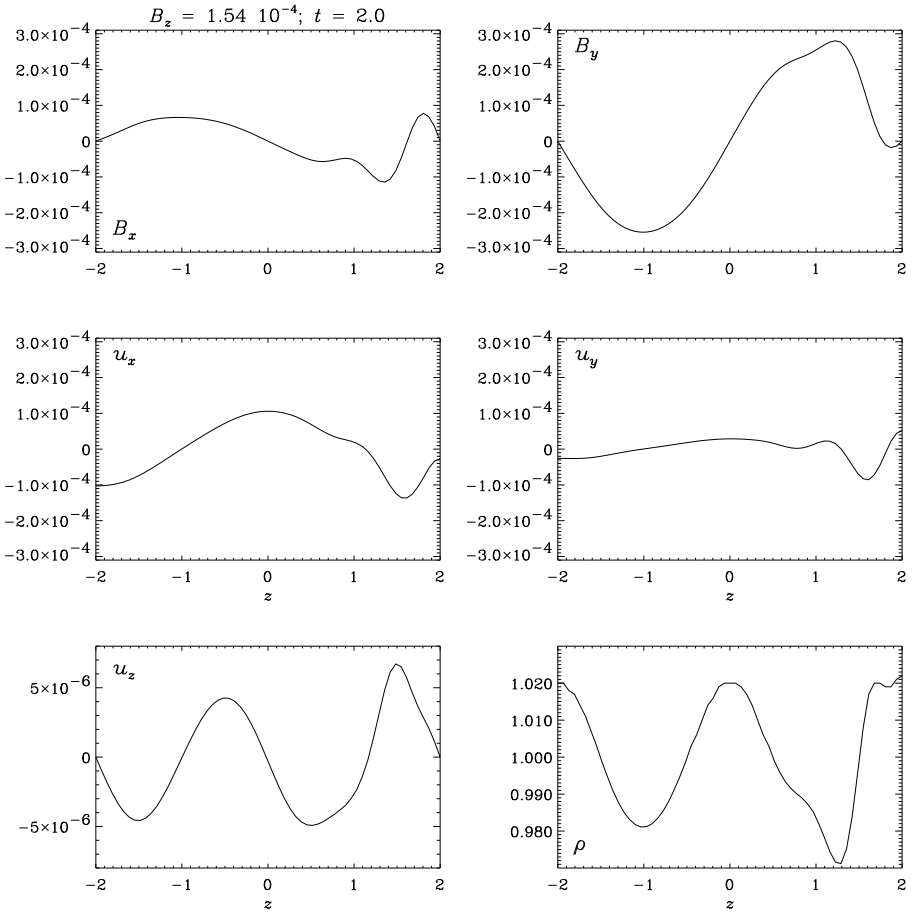

Fig. 6. The evolved state of Model 3 at 2.0 orbital periods. The figure is organised in the same way as Fig. 4

dependence is not described by $\exp(ik_z z)$. It is possible to re-write Eq. (2) as a set of second-order ordinary differential equations in the Lagrangian displacement, ξ (Gammie &Balbus 1994). Restricting ourselves as before to an imposed vertical field and modes with no dependence on the horizontal coordinates, we find

$$B^2 \frac{\mathrm{d}^2 \xi_x}{\mathrm{d}z^2} = -\left(\omega^2 + 3\Omega_0^2\right) \rho \xi_x + 2i\omega\Omega_0 \rho \xi_y, \tag{29}$$

and

$$B^2 \frac{\mathrm{d}^2 \xi_y}{\mathrm{d}z^2} = -2i\omega\Omega_0 \rho \xi_x - \omega^2 \rho \xi_y, \tag{30}$$

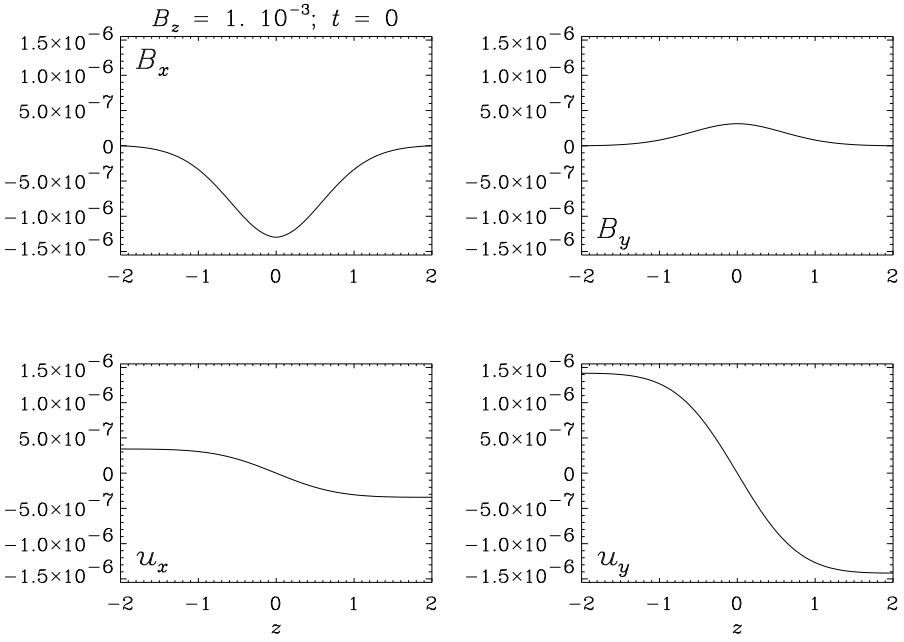

Fig. 7. The initial state of Model 4. The imposed vertical magnetic field is $1\,10^{-3}$, the density profile is a Gaussian with a maximum of 1.0, and the angular velocity is 10^{-3} (as in the unstratified models). The figure is organised in the same way as Fig. 2

with the boundary conditions

$$\frac{\mathrm{d}\xi_x}{\mathrm{d}z} = \frac{\mathrm{d}\xi_y}{\mathrm{d}z} = 0 \ \text{ at } \ z = \pm 2H. \tag{31}$$

We calculate a set of eigenmodes using a shooting method, and normalise them such that $|\xi_x| = 1$ at $z = \pm 2H$. These eigenmodes are then orthogonal, and we can calculate $\delta\mathbf{u}$ and $\delta\mathbf{B}$ from them as

$$\delta\mathbf{u} = -i\omega\boldsymbol{\xi} + 2A\xi_x\mathbf{e_y}, \tag{32}$$

and

$$\delta\mathbf{B} = B\frac{\mathrm{d}\xi}{\mathrm{d}z}. \tag{33}$$

Our models are described briefly in Tab. 2. The wavelength is no longer a well-defined concept, so we prefer to identify the modes by the number of nodes in the velocity perturbation, N_{nodes}.

In Model 4 the magnetic field is so strong that the only unstable mode is the one with $N_{\mathrm{nodes}} = 1$ (Fig. 7). Furthermore the growth rate of this mode is

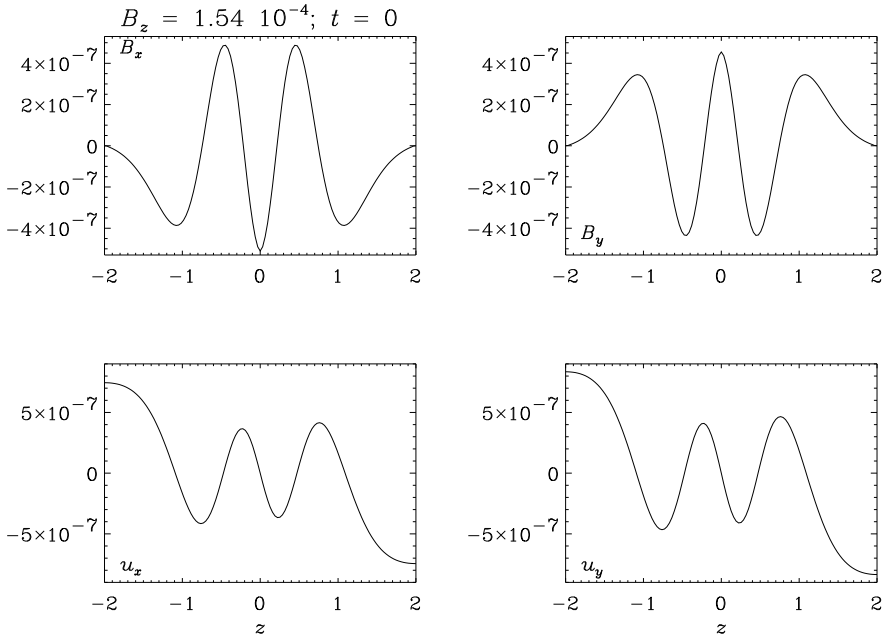

Fig. 8. The initial state of Model 5. The imposed vertical magnetic field is $1.54\,10^{-4}$. The figure is organised in the same way as Fig. 2

Table 2. Vertical eigenmodes in isothermal, stratified discs. For each model we give the number of grid points used, N_z, the imposed vertical magnetic field, B, the number of nodes in u_x, $N_{\rm nodes}$, and the growth rate, σ, in units of the Keplerian angular frequency

Model	N_z	B	$N_{\rm nodes}$	σ
4	127	$1\,10^{-3}$	1	0.34
5	127	$1.54\,10^{-4}$	5	0.75
6	127	$1.54\,10^{-4}$	1	0.38
7	127	$2\,10^{-4}$	5	0.64

significantly smaller than the maximal growth rate, $0.75\Omega_0$, which can only be achieved by fine-tuning the magnetic field strength to make an appropriate mode fit precisely in the disc. An imposed magnetic field of $1.54\,10^{-4}$ gives close to the maximum growth rate for a $N_{\rm nodes} = 5$ mode (Fig. 8). At this field strength there is a large range of unstable modes. An interesting alternative is therefore to excite the $N_{\rm nodes} = 1$ mode (Fig. 9). The $N_{\rm nodes} = 3$ mode is growing more rapidly than the originally excited mode, and can be distinguished in a snapshot

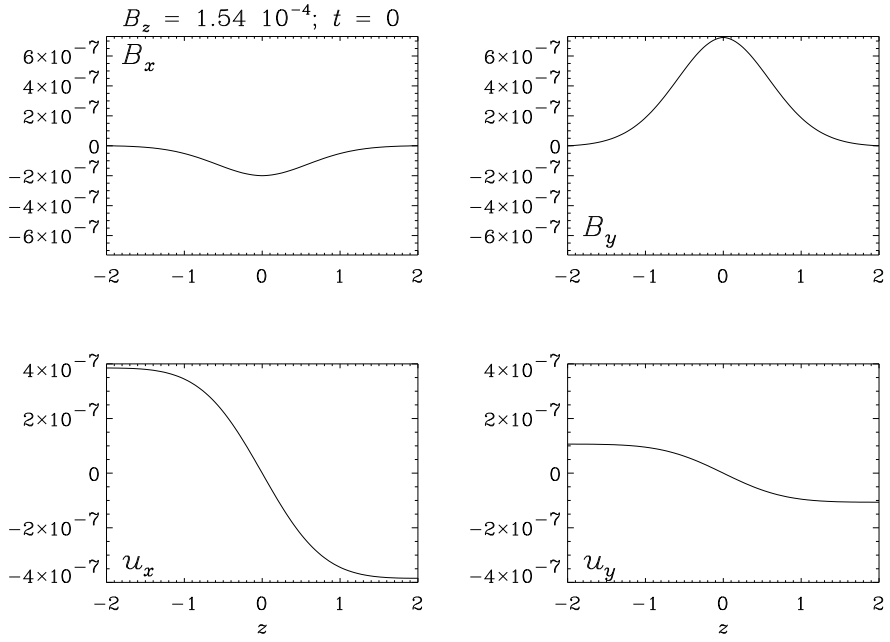

Fig. 9. The initial state of Model 6. The imposed vertical magnetic field is $1.54\,10^{-4}$. The figure is organised in the same way as Fig. 2

at 2.4 orbital periods (Fig. 10). At around this time the growth rates of, in particular, B_x and u_y increases from 0.37 to 0.67 (Fig. 11), which is close to the growth rate for the $N_{\rm nodes} = 3$ mode, which is 0.69. At 3.0 orbital periods the $N_{\rm nodes} = 3$ mode is dominating, and there may be a hint of an $N_{\rm nodes} = 5$ mode too (Fig. 12). We see also that the density maxima are located at the nodes of the horizontal magnetic field as predicted by Goodman & Xu (1994).

It can be instructive here to decompose the evolved state in the linear eigenmodes. We calculate the scalar product of u_x with the corresponding velocity of the eigenmode $u_{x,i}$ as

$$a_i = \frac{\int u_x u_{x,i} \rho {\rm d}z}{\int u_{x,i}^2 \rho {\rm d}z}, \tag{34}$$

where the integrals are taken over the entire vertical extent of our box, and ρ, taken at $t = 0$ works as a weighting function. The time evolution of the amplitudes a_i are plotted in Fig 13. Initially all modes are growing exponentially with their linear growth rates, but a_5 changes sign at 2.7 orbital periods. Note that the normalisation of the eigenmodes is arbitrary, and therefore the amplitudes of the different modes should not be compared with each other. It is intriguing that a_5 changes sign at the same time as u_x changes sign on the boundaries.

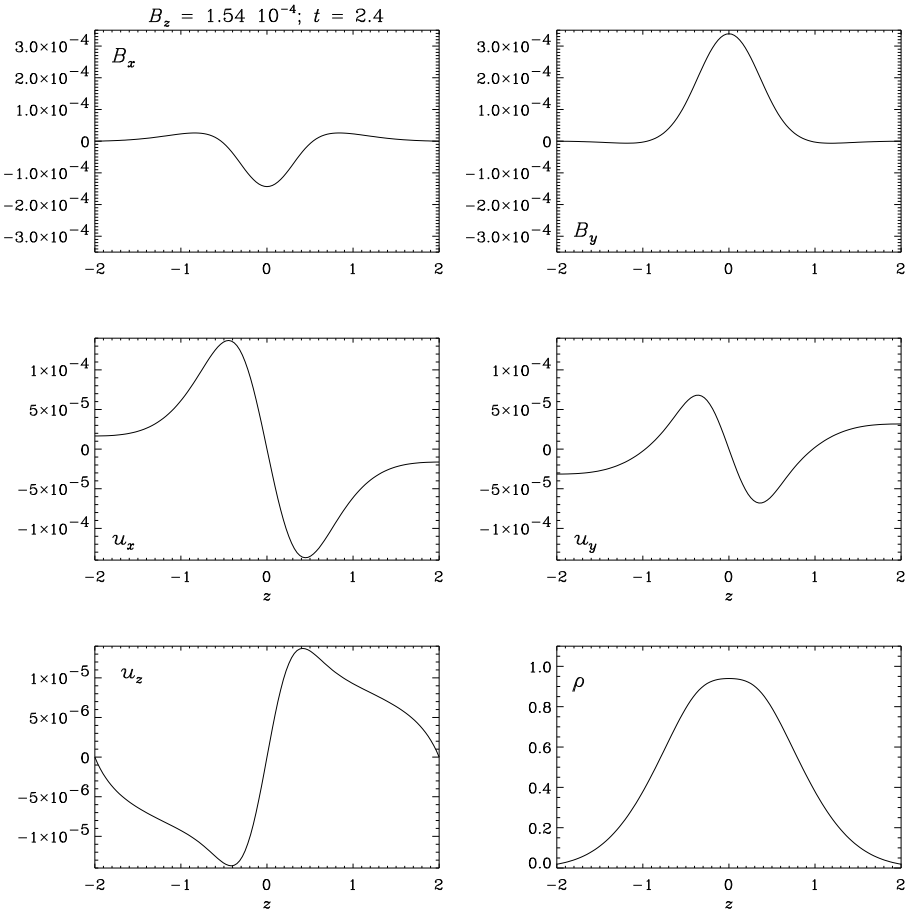

Fig. 10. The evolved state of Model 6 at 2.4 orbital periods. The figure is organised in the same way as Fig. 4

Model 7 is the opposite to Model 6. Here we start out with the $N_{\rm nodes} = 5$ mode (Fig. 14) although the fastest growing mode is the $N_{\rm nodes} = 3$ mode. Comparing with the evolved mode after 3.4 orbital periods (Fig. 15) one may suspect that it has obtained some power in the lower odd modes. To investigate that we do a spectral decomposition including the first three odd modes (Fig 16). From the start all modes are growing exponentially at the expected growth rates, but at three orbital periods a_1 increases its growth rate to $2\Omega_0$, due to a nonlinear interaction between the modes.

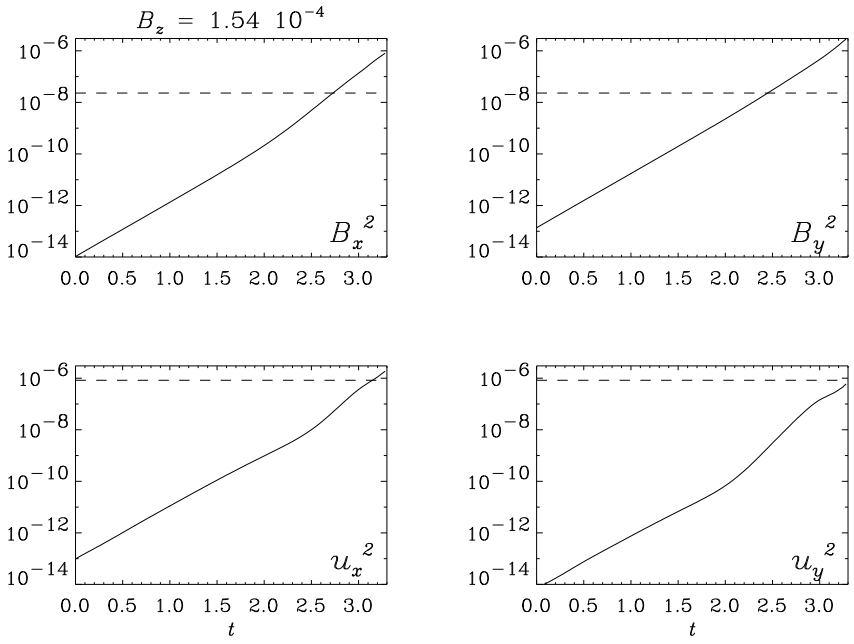

Fig. 11. The vertical averages of B_x^2 and B_y^2 (upper row), and u_x^2 and u_y^2 (lower row) as a function of time for Model 6. Time is given in orbital periods. The dashed lines denote B^2 (upper row) and c_s^2 (lower row)

5 Discussion and summary

In this paper we have been studying the nonlinear development of one-dimensional unstable modes of a vertical magnetic field in a Keplerian disc. The intention was to understand the development of turbulence in accretion discs, and in particular the saturation mechanism.

Our results show that starting from the fastest growing mode the instability grows exponentially at the linear growth rate until the magnetic pressure fluctuations are large enough to dominate over the gas pressure. This is not surprising in view of the result of Goodman & Xu (1994) that a single mode of the shearing instability is an exact solution of incompressible MHD. The parasitic instability, that was also found by Goodman & Xu (1994), is not applicable here as it needs a non-vanishing wave number in the horizontal plane. A mode different from the fastest growing mode is on the other hand unstable, as other modes with higher growth rates are generated by the nonlinear terms in the equations. These modes will eventually dominate.

Hawley & Balbus (1992) investigated the instability of a homogeneous vertical field in the two-dimensional meridional plane. An important difference is

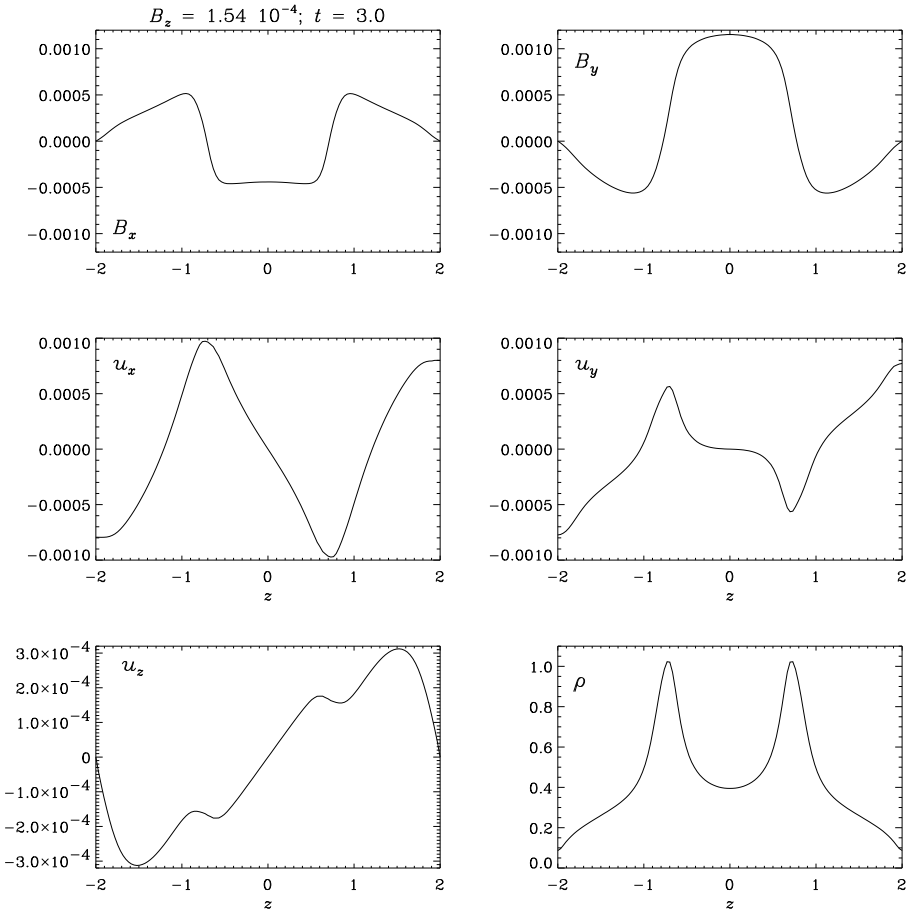

Fig. 12. The evolved state of Model 6 at 3.0 orbital periods. The figure is organised in the same way as Fig. 4

that as a perturbation they added random pressure fluctuations. As a result a large number of different modes were excited and grew with their own growth rates. By making a Fourier decomposition in the spatial coordinates they were able to determine the growth rates of each mode individually, and found that the modes initially followed the expected behaviour, but later on the growth rates decreased, and eventually the flow settled down to a so-called two-channel solution. The two-channel state appeared to be independent of the strength of the vertical field, and can thus not be interpreted as the dominating mode of the shearing instability, whose wavelength would have been a function of the magnetic field strength. As we do not find the two-channel solution in our simu-

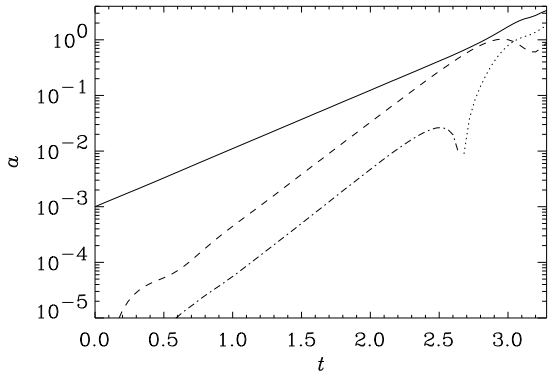

Fig. 13. The amplitudes of the first three odd eigenmodes as a function of time for Model 6. The lines represent a_1 (solid line), $-a_3$ (dashed line), a_5 (dashed-dotted line) and $-a_5$ (dotted line)

lations, we must conclude that it is a consequence of the two spatial dimensions. The two dimensions in themselves provide more freedom for dissipating magnetic fields, but equally important may be that the parasitic instability of Goodman & Xu (1994) becomes operative in two dimensions.

Both our one-dimensional results and the two-dimensional results of Hawley & Balbus (1992) are radically different from what has been found in three-dimensional simulations (e. g. Hawley et al. 1995, Brandenburg et al. 1995), as only the latter reach a turbulent state. It is of significant interest to understand the reason for these differences, as that may give us a clue to how the shearing instability leads to turbulence. The one- and two-dimensional simulations find a preferred length scale, in our case the wavelength of the most rapidly growing mode, and in Hawley & Balbus (1992) the length scale of the two-channel solution. In the case of the shearing instability of a toroidal magnetic field (e.g. Ogilvie & Pringle 1996, Terquem & Papaloizou 1996) the growth rate increases with increasing vertical wave number so that there is not a preferred length scale. This may explain why only three-dimensional models, which do allow the toroidal field to become unstable, develop a turbulent state.

Another important question is the nature of the saturation mechanism in the turbulent models. This work shows that the one-dimensional instability does not saturate until the magnetic pressure is comparable to the gas pressure. An attractive possibility for the three-dimensional models is that the field strength is limited by the magnetic field becoming buoyantly unstable, but the turbulence seems to saturate at comparable levels independently of whether the disc is stratified or not (Torkelsson et al. 1996). A more likely alternative is that the turbulence saturates when the magnetic field has become so tangled that the rate

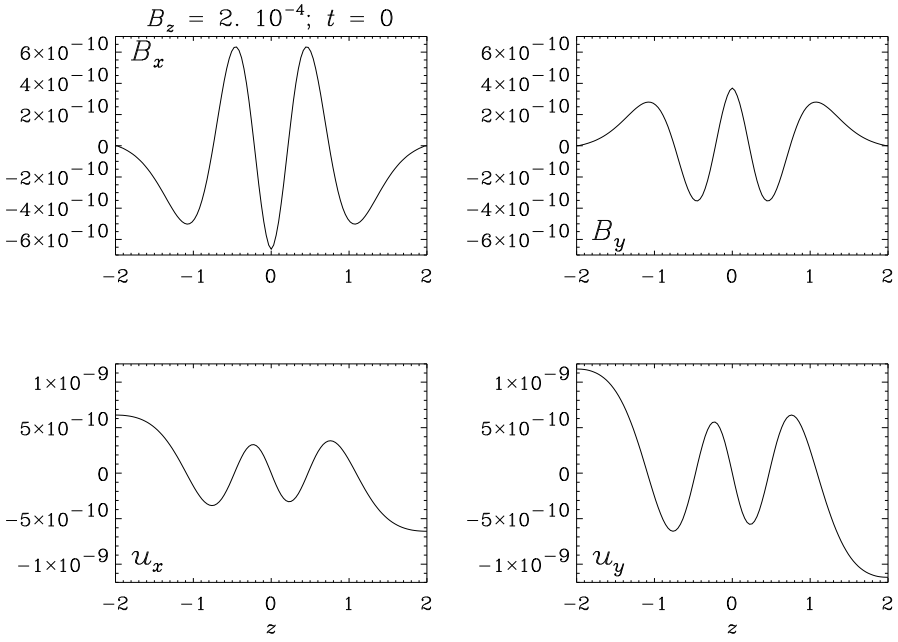

Fig. 14. The initial state of Model 7. The imposed vertical magnetic field is $2.\,10^{-4}$. The figure is organised in the same way as Fig. 2

of dissipation is comparable to the growth rate of the fundamental instabilities. This cannot happen in a system restricted to one dimension, and thus such a mechanism cannot work in the simulations described in this paper, but may work in three dimensions, where the magnetic field saturates at much lower field strengths.

In conclusion, we have studied the evolution of the shearing instability of a vertical magnetic field in a Keplerian disc in one dimension, the vertical. With these restrictions the instability does not saturate until the gas and magnetic pressures are comparable, and there is no turbulent cascade as the instability has a preferred mode with the maximum growth rate and a finite wave number.

Acknowledgement: UT is supported by an EU post-doctoral fellowship. This work was supported in part by the Danish National Research Foundation through its establishment of the Theoretical Astrophysics Center.

References

Balbus, S. A., Hawley, J. F., 1991, ApJ, 376, 214
Balbus, S. A., Hawley, J. F., 1992a, ApJ, 392, 662

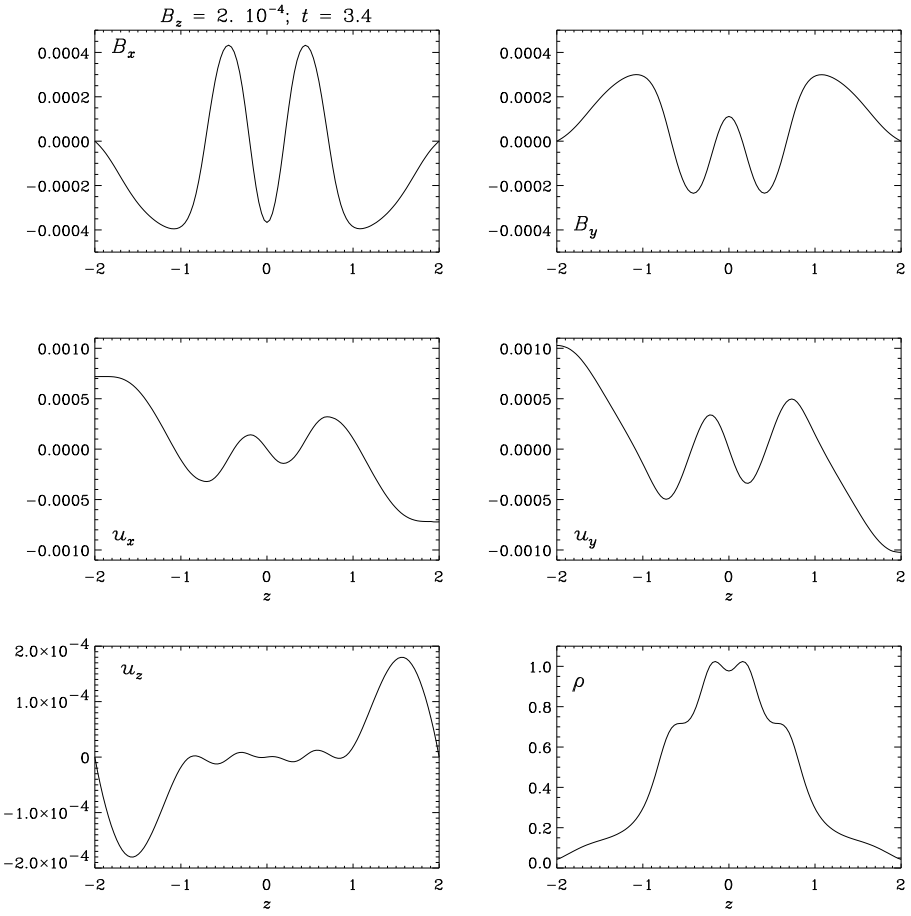

Fig. 15. The evolved state of Model 7 at 3.4 orbital periods. The figure is organised in the same way as Fig. 4

Balbus, S. A., Hawley, J. F., 1992b, ApJ, 400, 610
Brandenburg, A., et al., 1995, ApJ, 446, 741
Brandenburg, A., et al., 1996, ApJ, 458, L45
Chandrasekhar, S., 1960, Proc. Nat. Acad. Sci., 46, 253
Coleman, C. S., Kley, W., Kumar, S., 1995, MNRAS, 274, 171
Foglizzo, T., Tagger, M., 1995, A&A, 301, 293
Gammie, C. F., Balbus, S. A., 1994, MNRAS, 270, 138
Goodman, J., Xu, G., 1994, ApJ, 432, 213
Hawley, J. F., Balbus, S. A., 1992, ApJ, 400, 595
Hawley, J. F., Gammie, C. F., Balbus, S. A., 1995, ApJ, 440, 742
Hawley, J. F., Gammie, C. F., Balbus, S. A., 1996, ApJ, 464, 690

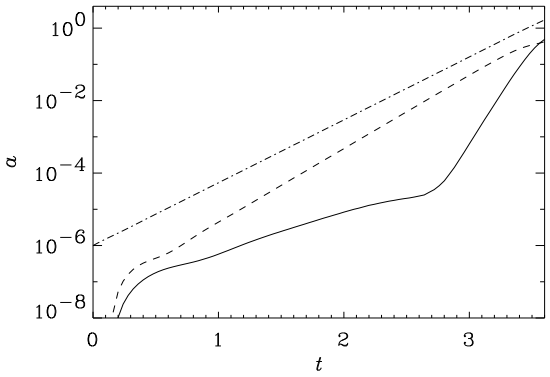

Fig. 16. The amplitudes of the first three odd eigenmodes as a function of time for Model 6. The lines represent $-a_1$ (solid line), a_3 (dashed line), a_5 (dashed-dotted line)

Matsumoto, R., Tajima, T., 1995, ApJ, 445, 767
Ogilvie, G. I., Pringle, J. E., 1996, MNRAS, 279, 152
Stone, J. M., et al., 1996, ApJ, 463, 656
Terquem, C., Papaloizou, J. C. B., 1996, MNRAS, 279, 767
Torkelsson, U., et al., 1996, Astrophys. Lett. & Comm., 34, 383
Velikhov, E. P., 1959, Sov. Phys. JETP. 9. 995